Non-Ergodic Probabilistic Seismic Hazard Analyses

M.A. Walling
Lettis Consultants International, INC

N.A. Abrahamson
University of California, Berkeley

SUMMARY
A method is developed that relaxes the ergodic assumption in probabilistic seismic hazard analysis (PSHA), accounting for the impacts on both the median and aleatory standard deviation of a ground-motion predication equation. Impacts on both intra- and inter-event residuals are addressed. The aleatory variability is separated from the systematic source, path and site effects using a strong motion data set from Taiwan with multiple recordings at each site and multiple earthquakes within small regions. Systematic site effects are accommodated by scale factors at individual sites. Systematic source- and path-effects are accommodated through models of their spatial covariance that are used to generate stochastic spatially correlated simulations of the path and source effects for applications to other regions with sparse data. Example hazard calculations show up to a factor of four increase in epistemic uncertainty without site-specific data.

Keywords: ergodic assumption, PSHA, spatial correlation effects, ground-motion prediction equations

1. INTRODUCTION

The present state-of-the-practice for performing a probabilistic seismic hazard analysis at a site makes an implicit assumption about the characteristics of the ground-motion over time; the assumption of stationarity. This is the ergodic assumption, and it is made in the probabilistic seismic hazard analysis when an empirical ground-motion model developed using recordings from multiple sites and from earthquakes from multiple regions is applied to a single site and single source location. This assumes that the variability in the ground-motion at a single site-source combination will be the same as the variability in the ground-motion seen in a typical strong motion data set containing recordings from different sites and from different sources at different source locations (Anderson and Brune, 1999). In this paper, we perform a probabilistic seismic hazard analysis relaxing the assumption of ergodicity, using the methodology developed that accounts for the complete epistemic (reducible) uncertainty and aleatory (irreducible) variability. Example non-ergodic probabilistic seismic hazard analyses are shown for two different cases: a site with recorded ground motion data and a site without recorded ground motion data.

2. COMPONENTS OF VARIABILITY IN GROUND MOTION

In most modern empirical ground-motion studies, the total variability is separated into inter-event and intra-event components to account for correlations of the recorded ground-motion from a single earthquake and to account for uneven sampling of the different earthquakes. Using the notation from Al Atik & Abrahamson (2008) the observed ground-motion is written as

$$y_{ik} = f\left(\overrightarrow{X_{\iota k}}, \overrightarrow{\theta}\right) + \xi_{ik} + \eta_i \tag{2.1}$$

where y_{ik} is the natural log of the ground-motion parameter, y_{ik} is the ground-motion model, $\overrightarrow{X_{ik}}$ is the vector of independent parameters (e.g., magnitude, distance, style-of-faulting, site condition), $\vec{\theta}$ is the vector of coefficients to be estimated by the regression and, ξ_{ik} and η_i are the intra-event and inter-event residuals for the kth site from the ith earthquake, respectively. The intra-event residuals, ξ_{ik}, include the effects of differences in the site amplification at the different sites and the effects of the differences in the path effects, while the inter-event residuals, η_i, capture the effects of differences in the average source properties for the different earthquakes in the data set. The standard deviations of the intra-event residuals, ξ_{ik}, and the inter-event residuals η_i, are σ and τ respectively, with the total standard deviation, σ_T written as

$$\sigma_T = \sqrt{\tau^2 + \sigma^2} \tag{2.2}$$

2.1 Components of the intra-event standard deviation

The intra-event residuals include the effects of differences in the site amplification at the different sites. If we have multiple recordings at each site, then we can separate out a median site-specific amplification term for each site, ξ_{S_k}, from intra-event term ξ_{ik} to estimate the residual term, ξ_{rik}. Parameter ξ_{S_k} is the inter-site residual for the kth site (representing the site-specific amplification factor) and ξ_{rik} represents the deviation of the record from the average site-specific amplification ξ_{S_k}. Similarly, if we have recordings from multiple earthquakes in a similar location, we can also separate out a median difference in the path effects from the ξ_{rik}. Using these steps, the intra-event residual can be partitioned as Eqn 2.3 and since, the standard deviations of these individual terms show very low correlation, and σ can be written as Eqn 2.4. In Eqn 2.3, ξ_{Pkl} is the path intra-event term at the lth location at the kth site, and ξ_{0ik} is the left-over remaining term of the ith source at the kth site. In Eqn 2.4, σ_s, σ_p, σ_0 is the standard error term of the site, path and left-over term, respectively.

$$\xi_{ikl} = \xi_{S_k} + \xi_{p_{kl}} + \xi_{0_{ik}} \tag{2.3}$$

$$\sigma = \sqrt{\sigma_S + \sigma_P + \sigma_0} \tag{2.4}$$

2.2 Components of the inter-event standard deviation

The inter-event residuals capture the effects of differences in the average source properties for the different earthquakes in the data set. If we have multiple recordings from a single source region, then we can separate out the median event term for each region and the inter-event residual can be written as Eqn 2.5 and the inter-event standard deviation can then be written as Eqn 2.6. In Eqn 2.5 parameter η_{SRl} is the source region inter-event term for the lth source location and η_{0i} is the remaining inter-event term and Eqn 2.6 parameter τ_{SR} and τ_0 is the standard deviation of η_{SRl} and η_{0i}, respectively.

$$\eta_{i,l} = \eta_{SR_l} + \eta_{0_i} \tag{2.5}$$

$$\tau = \sqrt{\tau_{SR}^2 + \tau_0^2} \tag{2.6}$$

2.3 Removing the epistemic uncertainty from the total standard deviation

The total standard deviation from a typical empirical ground-motion model can be written in terms of the components of the standard deviation defined earlier, as Eqn 2.7. The σ_S, σ_P, τ_{SR} components represent uncertainty that is epistemic in the median ground-motion for a single site and single-source location because each term represents the deviation of a systematic process that can be measured, given enough available ground motion recordings. Removing the three epistemic terms from σ_T, the aleatory part of σ_T is given by Eqn 2.8. Once these systematic and repeatable effects from the site, ξ_{Sk}, path, ξ_{Pkl}, and source, η_{SRl}, are separated out of the aleatory component of the ground motion

variability, data can be collect to constrain each term ξ_{Sk}, ξ_{Pkl}, and η_{SRl}, which can then be used to estimate a more accurate site-specific hazard. This is done by modifying Eqn 2.1 to Eqn 2.9. Eqn 2.9, is a site-source specific ground motion model, which accounts for the repeatable and systematic effects of the site, path, and source.

$$\sigma_T = \sqrt{\tau_{SR}^2 + \tau_0^2 + \sigma_S^2 + \sigma_P^2 + \sigma_0^2} \qquad (2.7)$$

$$\sigma_{SP} = \sqrt{\tau_0^2 + \sigma_0^2} \qquad (2.8)$$

$$y_{i,k,l} = f\left(\overrightarrow{X_{\iota,k,l}}, \overrightarrow{\theta}\right) + \xi_{S_k} + \xi_{p_{k,l}} + \xi_{0_{i,k}} + \eta_{SR_l} + \eta_{0_i} \qquad (2.9)$$

2.4 Results from previous studies

Previous studies by Chen and Tsai (2002), Atkinson (2006), Morikawa et al. (2008) and Lin et al. (2010) have estimated the reduction in σ_T for site-specific, site-specific path-specific, and site-specific region-specific effects. These studies have found that the modeling aleatory variability of ln(PGA) can be reduced by 10-40% for site-specific and by 40-70% for site-specific path-specific (Lin et al., 2011). The results from Lin et al. (2011) are summarized in Table 2.1

Table 2.1. Results from Lin et al (2011)

σ_T	τ	σ	σ_S	σ_r	σ_P	σ_0	τ_{SR}	τ_0	σ_{SS}	σ_{SP}
0.733	0.446	0.565	0.228	0.499	0.331	0.331	0.254	0.315	0.619	0.458

3. ESTIMATING THE SYSTEMATIC COMPONENTS

A site-specific source-specific ground motion model (Eqn 2.9) is required for every potential source when performing a PSHA that relaxes the ergodic assumption. This is achievable through models of GMPE parameters ξ_{Sk}, ξ_{Pkl}, and η_{SRl} that have been developed and constrained using data sets of ground motion records and/or of ground motion simulations. In practice, data sets of this type will most likely not be available, or at best, partially available at a particular site to constrain ξ_{Sk}, ξ_{Pkl}, and η_{SRl} terms with confidence. To proceed with relaxing the ergodic assumption, regions without data can use generic models of ξ_{Pkl}, and η_{SRl} developed with site-source specific datasets from regions with data as analogs and take the additional step to incorporate the additional epistemic uncertainty in the value of ξ_{Sk}, ξ_{Pkl}, and η_{SRl} terms into the PSHA.

Epistemic uncertainty in site term, ξ_{Sk}, is the easiest to address. It is not correlated to source parameters and the correlation of ξ_{Sk} to surrounding sites can be ignored because only a single site is assessed in a PSHA. Epistemic uncertainty in the path, ξ_{Pkl}, and source, η_{SRl}, terms is not as straightforward. These terms are correlated for closely spaced sources. The median ground-motion at a site from sources recorded at nearby locations should be more similar than sources recorded at far-way locations. Meaning, we expect that if one source is above average then another source located nearby should also tend to be above average due to systematic path and source region effects. Its degree of similarity dependent on the spatial proximity of the sources relative to one another, and the spatial proximity of the considered sources relative to the seismic hazard site.

Dealing with site-source specific GMPEs terms that are spatially correlated, the epistemic uncertainty in the estimates of each parameters should be incorporated through the logic tree in which the end-branch of the node contains an alternative spatial map of ξ_{Pkl} and η_{SRl} estimates. The source term η_{SRl} map would be a spatial grid of η_{SRl} estimates that are correlated by the spatial distance represented by the grid point spacings that is equivalent to the spatial distance separating two sources by ΔH_{ij}. Estimates of η_{SRl} of nearby grid points would be more correlated then the estimates of grid points

located further apart. Fig. 3.1a, is provided to illustrate this point. Source 1 and 2 will have more similarity in source effects than Sources 2 & 3 and 1 & 3 because ΔH_{12} is less than both ΔH_{23} and ΔH_{13}.

The path term ξ_{Pkl} map would be a spatial grid of ξ_{Pkl} estimates that are correlated by the epicentral azimuths θ_{ikj} of the source. Estimates of ξ_{Pkl} from sources that share a more similar path would be more correlated. Fig. 3.1b is provided to illustrate this point. Source 2 &3 share a more similar wave-path than Source 1 &4. Source 2 & 3 have a θ_{ikj} that is smaller even though the source separation distances ΔH_{23} and ΔH_{14} are the same and as such ξ_{Pkl} are more correlated.

(a)   (b)   (c)
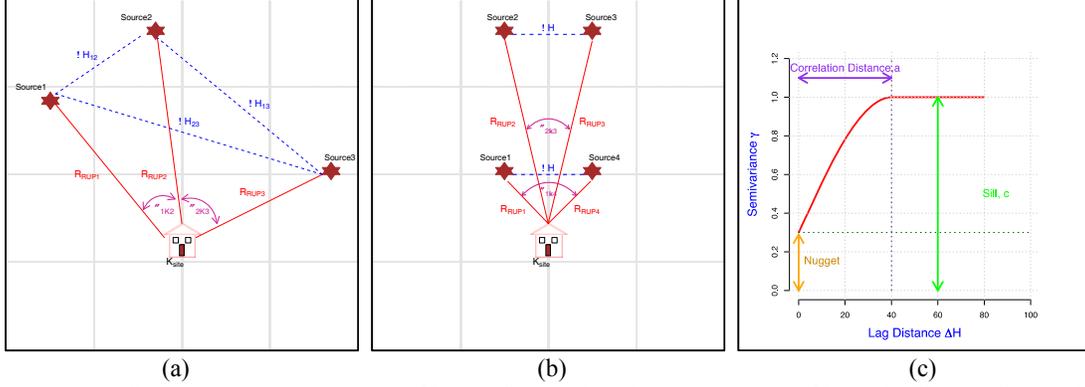
Figure 3.1. a) Source separation distance $\Delta H_{1,2}$ for Source 1 & 2 is shorter than $\Delta H_{1,3}$ and $\Delta H_{2,3}$ for Source 1 & 3, or Source 2 &3, respectively. The ground motion systematic source effects from Source 1 & 2 should display a greater correlation than systematic source effects for Source 1 & 3, or Source 2 &3; b) Source 2 &3 share more similar wave-paths and Source 2 & 3, even though ΔH is the same because the azimuthal difference $\theta_{2,3}$ is smaller than $\theta_{1,4}$. This leads to more correlated systematic path effects between Source 2 &3, than Source 1 & 4; c) an example semi-variogram plot illustrating the nugget, the sill c and the correlation distance α.

3.1. Spatial correlated logic trees

A summary of the procedure for developing spatially correlated logic trees is described here; a more detail explanation can be found in Walling (2009). This procedure uses techniques developed in the field of geostatistics that were created to describe the spatial covariance model of a physical process Z. In geostatistics, this is performed through the semi-variogram, γ_Z, function, which is directly related to the spatial covariance function through the following relationship,

$$\gamma_z(\Delta H) = Var[Z(h=0)] - C_z(\Delta H) \tag{3.1}$$

in which ΔH is the spatial measure of distance separating two points, $Var[]$, is the variance of the process when the spatial separation distance is equal to 0, and C_z is the spatial covariance model. The semi-variogram models are developed by calculating the empirical semi-variogram values and fitting these values to a closed form analytical semi-variance function that is known to be positive definite. A spherical semi-variogram function with parameters, c, α, and $nugg$, is shown in Fig 3.1c. The sill, c, is the semi-variogram value at which the semi-variogram reaches a limiting value, which occurs when processes $Z(x)$ and $Z(x+h)$ are uncorrelated. The range, α, is the correlation distance, the lag distance, h, at which $Z(x)$ and $Z(x+h)$ are uncorrelated, and the $nugg$ is the nugget effect which is the semi-variogram value at the zero separate distance.

The spherical semi-variance function is given by,

$$\gamma_z(h) = c \times Sph\left(\frac{h}{a}\right) = \begin{cases} c \times \left[1.5\left(\frac{h}{a}\right)^3 - 0.5\left(\frac{h}{a}\right)^3 + nugg\right] & , if\ h \leq a \\ c + nugg & otherwise \end{cases} \tag{3.2}$$

The *nugg* is then subtracted from its respective semi-variogram models γ_η and $\gamma_{\xi r}$ to estimate the semi-variogram source and path $\gamma_{\eta SR}$ and $\gamma_{\xi P}$ and using Eqn 3.1 the spatial covariance function of η_{SRl} and ξ_{rik} is indirectly determined

Spatial maps of correlated terms η_{SRl} and ξ_{Pkl} that account for additional epistemic uncertainty when the ergodic assumption is relaxed is created by applying the Fourier Integral Method (FIM) to the semi-variogram functions $\gamma_{\eta SR}$ and $\gamma_{\xi P}$. FIM is a spectral-simulation method that reproduces either the mean and the variance or the semi-variogram by using the spatial covariance models' spectral density representation in the wave-number domain to generate multiple realizations of the stationary process by randomizing the phase spectrum. In this methodology, the amplitude spectrum of the spectral density function is held fixed, producing stochastic realizations in the space domain that will have the second-order properties that are consistent with observations. The advantage of using FIM over the other methods that also generate realizations of random fields is that it is a fast and relatively simple method. The procedure of generating spatially correlated random fields using FIM is described in Walling (2009).

The semi-variogram model also has the advantage that it can be related back to the aleatory standard deviation components in the GMPE through the nugget parameter. The nugget is a measure of the aleatory variability in either η_{SRl} or ξ_{Pkl}. The aleatory standard deviation for the path terms, σ_0, can be estimated as Eqn 3.3. For the source term, a similar relation applies to calculate τ_0. Once both σ_0 and τ_0 are determined the single-station path-specific aleatory variability σ_{SP} can be computed using Eqn 2.8.

$$\sigma_0 = \sqrt{nugg_{\gamma\xi P}} \tag{3.3}$$

Our epistemic uncertainty in the values of ξ_{Pkl} and η_{SRl} will depend on the available ground motion data at the site. At a site with no ground-motion recordings, there will be large uncertainty in both parameters and, as previously discussed, we would move forward by using the observed spatially correlation of the known part of the systematic effects from a region that has been well recorded, as an analog for the expected spatial correlation in the target region (without available ground-motion recordings). The predictors of the generic models of ξ_{Pkl} and η_{SRl}, then represent the measure of our epistemic uncertainty. In this case, this leads to the same mean hazard whether we assume the ergodic assumption or if we remove the ergodic. The fractiles of the hazard will be different, with much broader fractiles for the hazard without the ergodic assumption than for hazard with the ergodic assumption. Having alternative semi-variogram models captures the epistemic uncertainty in the spatial correlation process itself. Alternatively, if there are ground-motion recordings at the site, the mean values of parameters ξ_{Pkl} and η_{SRl} can be estimated from the data. If it is found that the epistemic uncertainty is the same for the whole region, then standard methods can be used with a smaller covariance.

In the final scenario, which falls in-between these two latter extreme scenarios, where there are ground motion records available at the site from *some* earthquake sources, but not from *all* potential sources, then the methodology to incorporate the epistemic uncertainty is more complicated. In source locations where there are few, or no, ground motion records to constrain estimates of ξ_{Pkl} and η_{SRl}, the deviation of the simulated values from targeted values ξ_{Pkl} and η_{SRl} should reflect the large epistemic uncertainty from not having data to constrain these terms. Conversely, at the locations where there are data to constrain estimates of ξ_{Pkl} and η_{SRl}, the deviation of the simulated values from the average values should be reduced to reflect the reduced epistemic uncertainty. If FIM method is used, then random phase angles cannot be used to create stochastic spatially correlated maps. Instead, the phase should be selected to adjust for the non-stationary information. This method will be presented in a future paper.

Following the procedure describe above, multiple realizations of the spatial distribution of η_{SRl} and ξ_{Pkl} are created, where each realization is a branch on the logic tree. Fig. 3.2 is provided as an illustration. The spatial correlations of these parameters are evaluated using data sets from regions with multiple recordings at each site are evaluated.
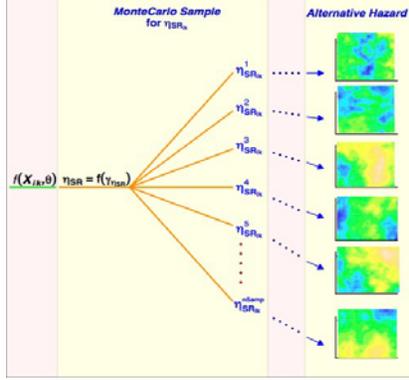
Figure 3.2. An illustration showing how the epistemic uncertainty of η_{SRI} is assimilated into hazard.

4.0 EXAMPLE

This section provides a demonstration of a PSHA with the ergodic assumption relaxed. The site-specific path-specific Taiwan data set from Lin et al. (2011) is used to quantify the spatial statistics of the systematic source and path effects and to quantify the size of the site terms. Lin et al (2011) estimated components η, ξ_{Sk}, and a intra-event record-to-record term, ξ_{rik}, for Taiwan using a strong motion data set consisting of 2004 recordings from 64 crustal earthquakes recorded at 84 sites. The sources were approximated as point sources, given by the hypocenter. The data set was restricted to ground-motions recorded on sites that had recorded at least 20 earthquakes. This requirement was placed to ensure a robust estimate of ξ_{Sk}. Most stations recorded between 20 and 26 earthquakes, and 12 stations recorded more than 30 earthquakes. The 1999 Chi-Chi mainshock was not included because of the complexities in defining the path for extended ruptures. The magnitude range of the remaining earthquakes spanned between $3.9M_w$ and $6.3M_w$. A description of the data-processing of the records can be found in Lin et al. (2011).

The spatial correlations of the source effects were quantified by performing a regression using the spherical semi-variogram function and the computed experimental semi-variogram η from the data set. The experimental semi-variogram was computed using the differences in the source effects for the ith and j^{th} source as a function of the source separation distance ΔH_{ij}, bins of 10 kms. The parameters estimated in the regression, $nugg$, α, and c, are listed in Table 4.1. Separating the systematic source effects from the aleatory variability, the nugget value was subtracted from $\gamma\eta$ to estimate the semi-variance of the source effects ($\gamma\eta_{SR}$) that capture the spatial correlation of the systematic source effects η_{SRl} within the Taiwan dataset.

As previously discussed, the spatial correlations of systematic path terms ξ_{Pkl} are a function of the separation angle, θ_{ikj}, between the ith and j^{th} source given the location of the kth site, and not just the source pair separation distance, ΔH_{ij}. To accommodate this type of correlation, multiple experimental semi-variograms were estimated from the data set, where each semi-variogram represents the spatial correlations from a different source-site R_{RUP}, distance bins of: 0 - 10, 10 - 20, 20 - 30, 30- 40, 40 - 50, 50 - 75, 75 - 100, and 100 - 110 km. Using the semi-variogram sphere model, a regression was performed and the semi-variogram parameters, $nugg$, α and c from each experimental semi-variogram was determined. The following smoothed models of the individual parameters α and c as a function of R_{RUP} were developed with these estimates,

$$\alpha = \overline{R_{rup}} \ln\left(a_1\overline{R_{rup}} + exp(1.0)\right) \tag{4.1}$$

$$c = \frac{c_1}{\ln\left(\overline{R_{rup}} - 1 + exp(1.0)\right)} \tag{4.2}$$

Eqns 4.1 and 4.2 allowed for a continuous semi-variogram model that changes as a function of the R_{RUP} distance. This semi-variogram is characteristic of a non-stationary semi-variogram because the spatial correlations are dependent on more than the lag distance, (ΔH_{ij}).

The maps of ξ_{Pkl} were developed in two stages, where the center of the map grid was defined as the reference station location. In the first stage, a stochastic simulation of ξ_{Pkl} was created using the FIM approach that reproduced the spatial correlations of semi-variogram model for R_{RUP} equal to 100-110 km. In the second stage, the non-stationary filter,

$$
\begin{aligned}
NSSF &= F_1 * F_2 \\
F_1 &= \begin{cases} f1 & if\ f1 \geq 0 \\ 0 & otherwise \end{cases} \\
F_2 &= \begin{cases} f2 & if\ f1 \geq 0 \\ 0 & otherwise \end{cases}
\end{aligned}
\qquad
\begin{aligned}
f1 &= \begin{cases} 1 - 1.5\left(\frac{\Delta H}{10}\right)^{0.5} + 0.5\left(\frac{\Delta H}{10}\right) & if\ \frac{\Delta H}{2} \leq 10 \\ 0 & otherwise \end{cases} \\
f2 &= \begin{cases} 1 - 1.5\left(\frac{\Delta H}{R_{rup}}\right)^{0.5} + 0.5\left(\frac{\Delta H}{R_{rup}}\right)^{2.5} & if\ \frac{\Delta H}{2} \leq R_{rup} \\ 0 & otherwise \end{cases}
\end{aligned}
\tag{4.3}
$$

was applied to the stochastic simulation to produce the spatial dependency that is characteristic to the non-stationary semi-variogram of ξ_{Pkl}. At each grid point of the map, the ξ_{Pkl} value was calculated as the weighted sum of ξ_{Pkl} values from nearby locations. The distance between the center grid location (i.e. station location) and every-other grid point location determined the weights used in the smoothing filter. The end-result of stage two is a spatial map of ξ_{Pkl} that reproduces the non-stationary semi-variogram model is created. The details of the non-stationary filter are given in Walling (2009).

For this example, the case with nearby low activity faults and more distant high activity faults was considered. A plan view map illustrating the site-source layout is seen in Fig. 4.1. To include the impacts of the differences in the ray paths, faults were located on both sides of the site. The source parameters summarizing: faults length, fault width, source mechanism, closest distance (R_{RUP}), slip-rate and mean magnitude are shown in Table 4.2 for each fault. Parameters: slip-rate and mean magnitude, have three alternative values that are considered credible. The weights of each branch, representing the credibility of the values, are provided in Table 4.2, shown in parenthesis. The epistemic uncertainty of these source parameters is typical for faults in California.

The example non-ergodic probabilistic seismic hazard analyses are shown for two different cases: one for a site without ground motion data available (Scenario A) and one for a site with ground motion data (Scenario F). These two different cases are compared to a third case, when the probabilistic seismic hazard analysis was run assuming the ergodic assumption (Ergodic case). For the Scenario A, we assume that there is no site-specific ground motion recordings available to constrain source and path terms, ξ_{Pkl} and η_{SRl}. The standard deviation of the systematic source effects ($\tau_{SR} = 0.28$) was determined by taking the square-root of its sill value minus the nugget value (0.078), listed in Table 4.3; the standard deviation of the systematic path effects ($\sigma_P = 0.42$) used in the hazard analysis was determined using the spatial map of ξ_{Pk} for source-site distances, R_{RUP}, less than 80 km. For Scenario F, we assume that site-specific information is available to constrain terms, ξ_{Pkl} and η_{SRl}, in particular, that all sources have two observations so the standard error of the mean is epistemic parameter value divided by the square-root of two. Making $\sigma_P = 0.29$ and $\tau_{SR} = 0.2$.

For Scenario A, we assume that there is also no site-specific information available to constrain the site term, ξ_{Sk}. The standard deviation of the site term, σ_S, used here, is the site term standard deviation reported by Lin et al. (2011) of 0.3. In contrast to this, Scenario F is assumed to have multiple site-specific recordings available, so that the uncertainty of ξ_{Sk} is negligible and σ_S is taken as 0. For both scenarios, ξ_{Sk} is taken as 0.15. The total standard deviation of the aleatory variability of the source and path (σ_{SP}) is the square-root of the sum of the nugget values (0.0688 for source; 0.114 for the path) and

equals 0.43. The total standard deviation (σ_T) was computed with Eqn 2.8. The four NGA ground motion models that include VS_{30} as a site parameters are considered: Abrahamson and Silva (2008); Boore and Atikinson (2008); Campbell and Bozorgnia (2008); Chiou and Youngs (2008). These four models are given equal weight.

For the non-ergodic case, the probability of exceeding the ground motion becomes

$$P\big(Sa > z \big| m, r, l, k, \eta_{SR_l}, \xi_{P_{kl}}, \xi_{S_k}\big) = 1 - \varphi\left(\frac{\ln(z) - \big(\hat{y}(m,r) + \eta_{SR_l} + \xi_{P_{kl}} + \xi_{S_k}\big)}{\sigma_{sp}}\right) \qquad (4.4)$$

To compute the non-ergodic hazard, the hazard code (HAZ42) developed by Abrahamson and Gregor (2009, personal communication) was modified to develop the maps of the spatially correlated ξ_{Pkl} and η_{SRl} terms and to include the site term, ξ_{Sk}. Before beginning the hazard run, a suite of maps of the ξ_{Pkl} and η_{SRl} terms are developed, representing the epistemic uncertainty in these two factors. For each map of values, the hazard is computed at the site. That is, the same map of values is used for all faults in a single realization of the hazard. The process was then repeated for 500 total realizations of the ξ_{Pkl} and η_{SRl} maps. For the site term, the process is easier because it is a single value. The site term is estimated and multiple realizations are implemented (one for each realization of the ξ_{Pkl} and η_{SRl} maps) to represent the epistemic uncertainty in the site factor. In this example, only a constant site factor is used, so differences in the non-linear site response are not considered.

The range of the fractile values of the computed hazard characterizes the range of epistemic uncertainty. In the first case, we compare the mean and fractiles of the hazard using the ergodic assumption and Scenario A, shown in Fig. 4.2a. For the ergodic assumption, the 10-90% range at 0.4g is 1.4. For Scenario A, this range increases to 19.9. The total range of increase in the epistemic uncertainty for this comparison is the ratio of the listed ranges, which at 0.4 g is a factor of 13.9 increase. In Scenario F, when previous estimates of the site (ξ_{Sk} = 0.15), source and path effects are available, the computed mean hazard and fractiles will best approximate the hazard at the site. For this case, we have combined two previous estimates of the path and source spatial correlations to compute my initial estimate of the systematic effects, shown in Fig. 4.2b. The comparison of the computed mean hazard and 0.1, 0.5 and 0.9 fractile values are shown in Fig. 4.2b. The sill values for the systematic effects were reduced to 0.231 and 0.039 for the path and source effects, respectively, to reflect a 50% reduction on the standard deviation σ_P and τ_{SR}. The mean hazard is approximately the same; however, because the path effects are non-stationary, the mean hazard does not have to be equal. The range of the 10-90% fractile range is at 0.4 g for Scenario F is a factor of 6.6. The increase in epistemic uncertainty for Scenario 2 compared with the ergodic case at 0.4 g is a factor of 3.2.

5.0 CONCLUSION

If the ergodic assumption is made, then there is no difference between the ground motion for earthquakes with the same magnitude and same distance, but there will be differences in the different directions away from the site. With two identical faults located on either side of the site, the hazard curves from the pairs of similar faults would be identical. For the non-ergodic case, the hazard curves can be different from these pairs of similar faults. It is important to note that removing the ergodic assumption does not always lead to a reduction in the estimate of the hazard. If the median ground-motion, $f(\vec{X}_{ik}, \vec{\theta})$, for the controlling source shown is higher than the regional median, $f(\vec{X}_{ik}, \vec{\theta})$ then the computed hazard will also be higher for a range of return periods. At very long return periods, the impact of the reduction in the modeling aleatory standard deviation may overcome the impact of the increase in the median and the hazard would then be reduced.

Although the mean hazard may be unchanged, the advantage of removing the ergodic assumption are several: it provides a framework for future studies to collect the data that will constrain the median model and reduce the modeling epistemic uncertainty in the median ground-motion; it shows the

benefits of a site-specific site response; it shows the benefits of region specific wave propagation numerical simulations; and it shows the benefits of installing instrumentation to record site-specific data to calibrate and validate models. Each is beneficial because each will provide some constraints on the epistemic uncertainty in the median site/source-specific attenuation and thereby reduce the epistemic uncertainty in the hazard.

Table 4.1. Coefficients value s of semi-variogram ξ_P and η_{SR} parameters

	a	c	nugget
ξ_P	-0.0092	0.462	0.114
η_{SR}	66	0.078	0.0668

Table 4.2. Source characterization for fault sources (Values in parentheses are the weights of the branches of the logic trees)

	Length (km)	Width (km)	Mechanism	Closest Distance (km)	Slip-rate (mm/yr)	Mean Characteristic Magnitude
Fault 1 & Fault 2	40	15	SS	10	0.15 (0.2) 0.30 (0.6) 0.6 (0.2)	6.5 (0.2) 6.7 (0.6) 6.9(0.2)
Fault 3 & Fault 4	100	15	SS	60	3.0 (0.2) 5.0 (0.6) 7.0 (0.2)	7.3 (0.2) 7.5 (0.6) 7.7 (0.2)

Table 4.3. Summary of non-ergrodic PSHA scenarios run

Parameter	σ_T	σ_P	σ_S	τ_{SR}	Obs. of ξ_P &η_{SR}	Obs. of ξ_S	Sill of ξ_P	Sill of η_{SR}
Ergodic	0.73	0.42	0.3	0.28	No	No	N/A	N/A
Scenario A	0.73	0.42	0.3	0.28	No	0.15	0.462	0.078
Scenario F	0.73	0.29	0.0	0.2	Yes	0.15	0.231	0.039
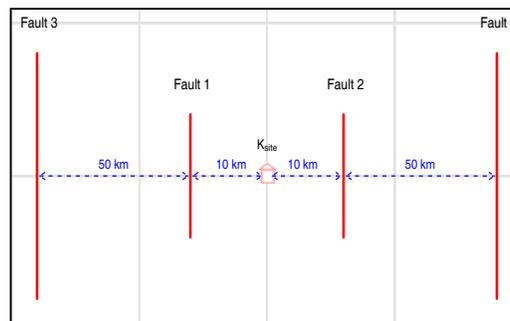
Figure 4.1. Map view showing the relative location of the four faults and site scenario. The nearby faults are low activity faults and the more distant faults are high activity faults. This site-source scenario was chosen to include the impacts of the differences in the ray paths, by locating the high and low activity faults on each side of the site'

Comparison of Ergodic Vs Scenario A   (a)

Comparison of Ergodic Vs Scenario F   (b)
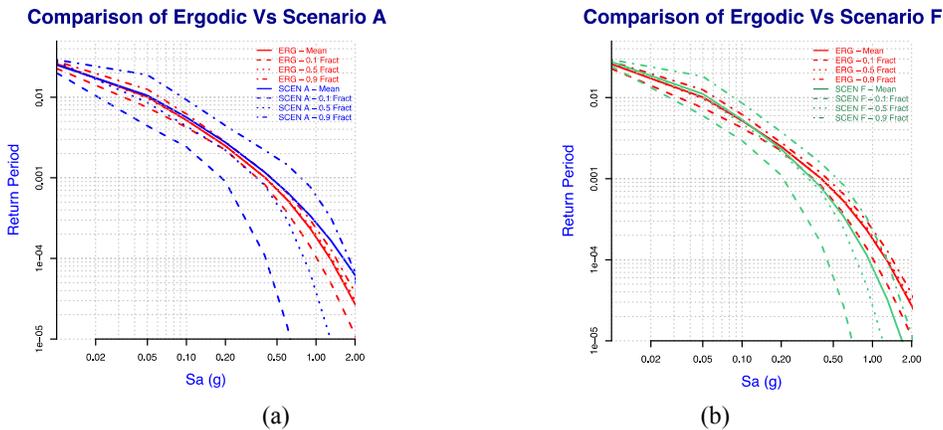
Figure 4.2. A comparison of results: mean hazard and fractils 0.1, 0.5 and 0.5 from running case Ergodic and a) Scenario A, information on the systematic effects for this site was not available. Scenario A assumes partially correlated systematic effects where sill value of the path and source were 0.462 and 0.078, respectively and σ_{SP} =0.43. Ergodic case assumes independent systematic effects σ_T=0.73; and b) Scenario F that had information on the site ξ_S=0.2 and σ_S = 0.15 and also assumes partially correlated systematic effects where sill value of the path and source were 0.231 and 0.039, respectively and σ_{SP} =0.43.

REFERENCES

Abrahamson, N.A., & Silva, W. (2008). Summary of the Abrahamson and Silva NGA ground-motion relations. *Earthquake Spectra*. **24**, 67-97.

Anderson, J.G., & Brune, J.N. (1999). Probabilistic seismic hazard analysis without the ergodic assumption. *Seismological Research Letters*. **70**, 19-28.

Atkinson, G. J. (2006b). Single-station sigma. *Bulletin of Seismological Society of America*. **96**, 446–455.

Al Atik, L. & N.Abrahamson. (2008). Nonlinear site response effects on the standard deviation of predicted motions. *Bulletin of Seismological Society of America*. **100**, 1288-1293.

Boore, D. M., & Atikinson, G.M. (2008). Ground-motion prediction equations for the average horizontal component of PGA, PGV, and 5%-damped PSA at spectral periods between 0.01s and 10.0s. *Earthquake Spectra*. **24**, 99–138.

Campbell, K. W., & Bozorgnia,Y (2008). NGA ground motion model for the geometric mean horizontal component of PGA, PGV, PGD and 5% damped linear elastic response spectra for periods ranging from 0.01 to 10 s. *Earthquake Spectra*. **24**, 139–171.

Chen, Y.-H., & Tsai, C.-C. (2002). A new method for estimation of the attenuation relationship with variance components. *Bulletin of Seismological Society of America*. **92**, 1984–1991.

Chiou, B., & Youngs, and R. R. (2008). Chiou-Youngs NGA ground motion relations for the geometric mean horizontal component of peak and spectral ground motion parameters. *Earthquake Spectra*. **24,** 173–215.

Idriss, I. M. (2008). An NGA empirical model for estimating the horizontal spectral values generated by shallow crustal earthquakes. *Earthquake Spectra*. **24**, 217–242.

Lin, P., Chiou, B., Abrahamson, N. A., Walling, M., Lee, C.-T. , & Cheng, C. (2011). Repeatable path effects on the standard deviation for empirical ground motion models. *Bulletin of Seismological Society of America*. **101**, 2281–2295.

Morikawa, N., Kanno, T., Narita, A., Fujiwara, H., Okumura, T., Fukushima, Y., & Guerpinar, A. (2008), Strong motion uncertainty determined from observed records by dense network in Japan. *Journal of Seismology*. **12**, 529–546, doi:10.1007/s109 50-008-9106- 2.

Restrepo-Velez Luis, F., & Bommer, J. J. (2003). An exploration of the nature of the scatter in ground motion prediction equations and the implications for seismic hazard assessment. *Journal of Earthquake Engineering*. **7(S1***), 171–199.

Strausser, F. O., Abrahamson, N. A., & Bommer, J. J. (2009). Sigma: Issues, insights, and challenges. *Seismological Research Letters*. **80(1),** 40–56.

Walling, M.A. (2009). Non-ergodic probabilistic seismic hazard analysis and spatial simulation of variation in ground motion. Ph.D. University of California, Berkeley.